

Accretion in the Early Outer Solar System

Scott J. Kenyon

Harvard-Smithsonian Center for Astrophysics
60 Garden Street, Cambridge, MA 02138
e-mail: skenyon@cfa.harvard.edu

and

Jane X. Luu

Leiden Observatory
PO Box 9513, 2300 RA Leiden, The Netherlands
e-mail: luu@strw.leidenuniv.nl

to appear in

The Astrophysical Journal

ABSTRACT

We describe calculations of the evolution of an ensemble of small planetesimals in the outer solar system. In a solar nebula with a mass of several times the Minimum Mass Solar Nebula, objects with radii of 100–1000 km can form on timescales of 10–100 Myr. Model luminosity functions derived from these calculations agree with current observations of bodies beyond the orbit of Neptune (Kuiper Belt objects). New surveys with current and planned instruments can place better constraints on the mass and dynamics of the solar nebula by measuring the luminosity function at red magnitudes, $m_R \geq 28$.

Subject headings: solar system: formation – Kuiper Belt

1. INTRODUCTION

Several remarkable discoveries have renewed interest in solar system formation. Recent surveys have detected many small icy bodies beyond the orbit of Neptune (e.g., Jewitt & Luu 1993; Williams *et al.* 1995; Jewitt *et al.* 1996; Luu *et al.* 1997; Gladman & Kavelaars 1997; Chiang & Brown 1999). Assuming a geometric albedo of 4%, these Kuiper Belt objects (KBOs) have radii of 50–400 km; the derived size distribution implies a significant population of smaller objects. With semi-major axes of 40–50 AU and orbital inclinations of 0° – 30° , the orbits of known KBOs suggest an annulus of planetesimals formed *in situ* and left over from the planetary formation epoch (Holman & Wisdom 1993). The presumed structure of this annulus resembles the dusty disks recently discovered around several nearby stars (Smith & Terrile 1984; Aumann *et al.* 1984; Jayawardhana *et al.* 1998; Koerner *et al.* 1998; Greaves *et al.* 1998). Planets similar to those in our solar system have not been detected in any of these disks, but direct images and radial velocity measurements of other nearby stars already imply the existence of more than one dozen extra-solar planets of several Jupiter masses (Latham *et al.* 1989; Marcy & Butler 1996; Cochran *et al.* 1997; Noyes *et al.* 1997; DelFosse *et al.* 1998; for a review see Marcy 1999).

These discoveries challenge planet formation theories. Most theories presume that planets grow by accretion of small planetesimals in a gaseous circumstellar disk (Safronov 1969; Goldreich & Ward 1973; see also Lissauer & Stewart 1993, Boss 1997, and references therein). Hitherto, numerical studies have focused on the formation of the prototypical terrestrial and gas giant planets, Earth and Jupiter (Greenberg *et al.* 1978, 1984; Nakagawa *et al.* 1983; Ohtsuki *et al.* 1988; Wetherill & Stewart 1989, 1993; Barge & Pellat 1990; Ruden & Pollack 1991; Pollack *et al.* 1996; Weidenschilling *et al.* 1997). If the initial disk mass is comparable to the Minimum Mass Solar Nebula¹, these calculations often have difficulty producing objects similar to the known terrestrial or gas giant planets during the estimated disk lifetime of ~ 10 – 30 Myr (Pollack *et al.* 1996; Weidenschilling *et al.* 1997). This problem is exacerbated in the outer solar system, where numerical calculations yield formation times exceeding 100 Myr for 500–1000 km radius KBOs (Stern 1995, 1996; Stern & Colwell 1997a,b). KBOs must form on shorter timescales in parallel with Neptune. Otherwise, Neptune’s gravity increases the velocities of nearby planetesimals, including those in the inner Kuiper Belt, on timescales of ~ 10 Myr (Malhotra 1996). This process

¹ The Minimum Mass Solar Nebula has a surface density $\Sigma = \Sigma_0(R/R_0)^{-3/2}$, where Σ_0 is the surface density of solid material at $R_0 = 1$ AU. We adopt $\Sigma_0 = 45$ g cm⁻² (Hayashi 1981; see also Weidenschilling 1977; Bailey 1994). This definition yields a total mass of solids $M_0 \approx 100 M_E$ inside the orbit of Neptune ($R < 30$ AU) and $M_0 \approx 10 M_E$ in the inner part of the Kuiper Belt ($R = 32$ – 38 AU), where $1 M_E = 6 \times 10^{27}$ g is the mass of the Earth.

prevents the growth of KBOs with radii exceeding 100–200 km, because large velocities hinder agglomeration.

We recently began to consider KBO formation in the outer solar system using an evolution code that follows planetesimal growth in the annulus of a circumstellar disk. Initial results indicate that KBOs can form at 30–50 AU on timescales of 10–100 Myr in disks with 1–3 times the Minimum Mass Solar Nebula when collisional disruption of planetesimals is unimportant (Kenyon & Luu 1998; hereafter KL98). Further calculations with an algorithm that includes disruptive processes lead to similarly short timescales for a wide range of initial conditions (Kenyon & Luu 1999; hereafter KL99). Here, we briefly summarize these new results, compare the theoretical model with current observations, and make predictions for comparison with future observations of KBOs.

2. MODEL

Our accretion code is based on the particle-in-a-box method, where planetesimals are a statistical ensemble of bodies with a distribution of horizontal and vertical velocities about Keplerian orbits (Safronov 1969). We perform calculations for a single annulus of width Δa centered at a heliocentric distance a . We approximate the continuous distribution of particle masses with i discrete batches having particle populations $n_i(t)$ and total masses $M_i(t)$. The horizontal and vertical velocity dispersions are $h_i(t)$ and $v_i(t)$ (Wetherill & Stewart 1993). The average mass of a batch, $m_i(t) = M_i(t)/n_i(t)$, changes with time as collisions add and remove bodies from the batch. This procedure conserves mass and provides a statistical method to follow the growth of $\gtrsim 10^{20}$ small planetesimals into a few planets. Detailed n -body calculations confirm the basic features of particle-in-a-box calculations for the early stages of planet growth described here (Ida & Makino 1992; Kokubo & Ida 1996).

To evolve the initial size distribution in time, we calculate collision rates for the coagulation equation, determine the outcome of each collision, and compute velocity changes due to collisions and long-range gravitational interactions (see KL99). Each two-body collision can produce (1) merger into a single body with no escaping debris (very low impact velocity), (2) merger into a single body with escaping debris (‘cratering’; low impact velocity), (3) rebound with or without cratering (modest impact velocity), or (4) catastrophic disruption into numerous smaller bodies (high impact velocity). The collision outcomes depend on the ratio of the impact energy Q_f to the disruption energy Q_d of two colliding planetesimals (Greenberg *et al.* 1978; Wetherill & Stewart 1993; Davis *et al.* 1994). Collisions with $Q_f > Q_d$ disrupt planetesimals into many small fragments. Collisions with $Q_f < Q_d$ yield a merged planetesimal and some small fragments if the collision velocity V_c

exceeds the minimum velocity for cratering V_f . Collisions with $Q_f < Q_d$ and $V_c < V_f$ yield a merged planetesimal with no cratering debris. We use an energy-scaling formalism to compute Q_d as the sum of the intrinsic tensile strength S_0 and the gravitational binding energy (Davis *et al.* 1985, 1994). The intrinsic strength is the dominant component of Q_d for bodies with $r_i \lesssim 1$ km; gravitational binding dominates S_0 for larger bodies.

For each collision, a velocity evolution algorithm distributes the kinetic energy among the resulting bodies and then accounts for collisional damping, kinetic energy transfer during elastic collisions (“dynamical friction”), angular momentum transfer during elastic collisions (“viscous stirring”), and gas drag (Hornung *et al.* 1985; see also Wetherill & Stewart 1993; KL98). Dynamical friction tries to enforce equipartition of kinetic energy between mass batches; viscous stirring increases the velocities of all bodies. Gas drag removes objects from the annulus and reduces the velocities of small objects which are well coupled to gas in the disk.

We tested the code against analytical solutions and published numerical results (KL98, KL99). We reproduced previous calculations for accretion at 1 AU (Wetherill & Stewart 1993) and collisional disruption of pre-existing large KBOs at 40 AU (Davis & Farinella 1997). Our calculations match analytical solutions well when the mass spacing between successive batches, $\delta = m_{i+1}/m_i = 1.1$ – 1.4 . Numerical solutions lag the analytic results by $\sim 10\%$ when $\delta = 1.4$ – 2 . The timescale to produce objects of a given size increases with δ , because poorer resolution prevents growth of large objects (see KL98).

Table 1 lists basic input parameters. The input cumulative size distribution N_C has the form $N_C \propto r_i^{q_0}$, with initial radii $r_i = 1$ – 80 m. The total mass in the annulus is M_0 ; $M_0 \approx 10 M_E$ for a Minimum Mass Solar Nebula. All batches start with the same initial velocity. We tested a range of initial velocities corresponding to initial eccentricities of $e_0 = 10^{-4}$ to 10^{-2} , as is expected for planetesimals in the early solar nebula (Malhotra 1995). The adopted mass density, $\rho_0 = 1.5$ g cm $^{-3}$, is appropriate for icy bodies with a small rocky component. The fragmentation parameters – V_f , S_0 , Q_c , f_{KE} , c_1 , and c_2 – are adopted from earlier work. KL99 describe these parameters in more detail.

To provide observational constraints on the models, we note that the known Kuiper Belt population contains at least one body with a radius of ~ 1000 km (Pluto), and $\sim 10^5$ KBOs with radii $r_i \gtrsim 50$ km between 30–50 AU. The cumulative size distribution of known KBOs can be fitted with $N_C \propto r_i^{q_{obs}}$, with $q_{obs} = 3 \pm 0.5$ (Jewitt *et al.* 1998; see also Chiang & Brown 1999). Successful models should reproduce these observations on timescales comparable to (a) the estimated lifetimes of the solar nebula and gaseous disks surrounding nearby young stars, $\lesssim 10^7$ yr (Russell *et al.* 1996; Hartmann *et al.* 1998) and (b) the formation timescale for Neptune, $\lesssim 10^8$ yr (Lissauer *et al.* 1996).

3. NUMERICAL RESULTS

We separate the growth of KBOs into three regimes. Early in the evolution, frequent collisions damp the velocity dispersions of small bodies. These bodies slowly grow into 1 km objects on a timescale that is approximated by $\tau_{1 \text{ km}} \approx 8 \text{ Myr} (M_0/10M_E) (e_0/10^{-3})^{0.65}$. This linear growth phase ends when the gravitational range of the largest objects exceeds their geometric cross-section. This “gravitational focusing” enhances the collision rate by factors of 10–1000. The largest objects then begin a period of “runaway growth”, when their radii grow from $\sim 1 \text{ km}$ to $\gtrsim 100 \text{ km}$ in several Myr. During this phase, dynamical friction and viscous stirring increase the velocity dispersions of the smallest bodies from $\sim 1 \text{ m s}^{-1}$ up to $\sim 40 \text{ m s}^{-1}$. This velocity evolution reduces gravitational focusing factors and ends runaway growth. The largest objects then grow slowly to 1000+ km sizes on timescales that again depend on M_0 and e_0 . Column (5) in Table 2 lists timescales to form Pluto-size objects τ_P as a function of the input parameters M_0 , δ , e_0 , and q_0 .

Fig. 1 shows cumulative size distributions for a model with $M_0 = 10 M_E$, $q_0 = 3$, and $S_0 = 2 \times 10^6 \text{ erg g}^{-1}$. The shapes of these curves depend on two competing physical processes: (1) growth by mergers and (2) erosion by high velocity collisions. In this example, collisions result in growth because the velocity dispersion is less than the catastrophic disruption threshold. However, the collision velocity exceeds the cratering threshold V_f . Cratering adds debris to all low mass batches. Gas drag removes material from low mass batches ($r_i \lesssim 10 \text{ m}$), but is ineffective at removing larger objects. The size distribution thus becomes shallower at small masses. At large masses, mergers produce a group of growing planetesimals with a steep size distribution. Once gravitational focusing becomes effective, the largest of these objects ‘run away’ from the rest of the ensemble to produce a smooth power law with a maximum radius r_{max} . As the evolution proceeds, r_{max} increases but the slope of the smooth power law remains nearly constant.

The main features of these results depend little on the input parameters. All calculations produce two cumulative power law size distributions connected by a transition region having an ‘excess’ of planetesimals (the “bump” in the curves in Fig. 1). The characteristic radius of this transition region increases from 0.3 km at $e_0 = 10^{-4}$ to 3 km at $e_0 = 10^{-2}$. If fitted with a power law of the form $N_C \propto r_i^{-q_f}$ at small masses, the cumulative size distribution follows the predicted limit for collisional evolution, $q_f = 2.5$ (Dohnanyi 1969). We perform least-square fits to obtain q_f at larger masses; column (6) of Table 2 lists derived values for q_f along with the 1σ error. Column (7) lists the radius range for each fit. The results are surprisingly independent of the input parameters. We find the small range $q_f = 2.75\text{--}3.25$ for calculations with $M_0 = 1\text{--}100 M_E$, $e_0 = 10^{-4}$ to 10^{-2} , $q_0 = 1.5\text{--}4.5$, and $S_0 = 10 \text{ erg g}^{-1}$ to $3 \times 10^6 \text{ erg g}^{-1}$. This model result is consistent with the

observed slope, $q_{obs} = 3 \pm 0.5$ (e.g., Jewitt *et al.* 1998).

4. COMPARISONS WITH OBSERVATIONS

As shown in Table 2, several calculations meet the success criteria defined in §2. Annuli with $M_0 \gtrsim 10M_E$ produce Pluto-sized objects on short timescales, $\tau_P \lesssim 50$ Myr (for $e_0 \lesssim 10^{-3}$). Models with smaller initial masses or larger initial eccentricities form Plutos on longer timescales, $\tau_P \gtrsim 50$ Myr. Plausible ranges of other input parameters – such as q_0 , S_0 , and f_{KE} – yield $\pm 20\%$ variations about these timescales. The results are insensitive to V_f and other collision parameters (KL99).

The crosses in Figure 1 compare our calculations directly with several observational constraints. The cross at $r_i = 50$ km indicates the number of KBOs with $r_i \gtrsim 50$ km estimated from recent ground-based surveys (Jewitt *et al.* 1998; see also Chiang & Brown 1999); the one at $r_i = 10$ km shows limits derived from a single, controversial measurement with *Hubble Space Telescope* (*HST*; Cochran *et al.* 1995, 1998; Brown *et al.* 1997). The third cross plots limits at $r_i = 1$ km derived from theoretical attempts to explain the frequency of short-period comets from the Kuiper Belt (Davis & Farinella 1997; Duncan & Levison 1997; Levison & Duncan 1997). Our predictions agree with ground-based surveys at 50 km and theoretical limits at 1 km, but fall a factor of ~ 10 short of the *HST* measurement at 10 km.

To compare with observations in more detail, we predict the luminosity function (LF) of KBOs directly from the computed number distribution. We use a Monte Carlo calculation of objects selected randomly from the cumulative size distribution N_C . We assign each object a distance from the Sun d_\odot and a random phase angle β between the line-of-sight from the Earth to the object and the line-of-sight from the Sun to the object. This phase angle lies between 0° and a maximum phase angle that is distance-dependent. The distance of the object from the Earth is then $d_E = d_\odot \cos\beta - (1 + d_\odot^2 (\cos^2\beta - 1))^{1/2}$. We derive the red magnitude of this object from a two parameter magnitude relation for asteroids, $m_{R,KBO} = R_0 + 2.5 \log(t_1/t_2) - 5 \log r_{KBO}$, where R_0 is the zero point of the magnitude scale, r_{KBO} is the radius of the KBO, $t_1 = 2d_\odot d_E$, and $t_2 = \omega((1-g)\phi_1 + g\phi_2)$ (Bowell *et al.* 1989). In this last expression, ω is the albedo, and g is the slope parameter; ϕ_1 and ϕ_2 are phase functions that describe the visibility of the illuminated hemisphere of the object as a function of β . We adopt standard values, $\omega = 0.04$ and $g = 0.15$, appropriate for comet nuclei (Jewitt *et al.* 1998). The zero point R_0 is the apparent red magnitude of the Sun, $m_{R,\odot} = -27.11$, with a correction for the V–R color of a KBO, $R_0 = m_{R,\odot} + \delta(V-R)_{KBO}$. Observations suggest that KBOs have colors that range from roughly -0.1

to 0.3 mag redder than the Sun. We treat this uncertainty by allowing the color to vary randomly in this range.

The important parameters in the model LF are the distributions of input sizes (derived from the accretion calculations), distances, and orbital parameters. We assume KBOs are evenly distributed between “Plutinos,” objects in 3:2 orbital resonance with Neptune having semimajor axes of 39.4 ± 0.2 AU, and “classical” KBOs with semimajor axes between 42–50 AU. The distance parameters are set by observations (Jewitt *et al.* 1998). This distance distribution is different from the 32–38 AU adopted for the coagulation calculations. Several tests show that accretion results at 42–50 AU are identical to those at 32–38 AU, except that the timescale to produce Pluto-sized objects is 50%–100% longer. To compute the model LF from the Monte Carlo magnitude distribution of KBOs, we scale the mass in the 32–38 AU annulus to match the mass in a 42–50 AU annulus, add in an equal number of Plutinos, and divide by the sky area. The distribution of KBO orbital parameters is poorly known. We adopt circular orbits to derive magnitudes; the LF is insensitive to other choices. We assume orbital inclinations of $i = 0^\circ$ to 5° to compute the sky area, which is a compromise between the $i \approx 0^\circ$ – 5° of classical KBOs and the $i \approx 10^\circ$ – 30° of Plutinos. The model LFs scale inversely with $\sin i$.

Figure 2 compares several models with the observed LF. The left panel shows models with $e_0 = 10^{-3}$ and different masses; the right panel shows models with the mass of a Minimum Mass Solar Nebula and different e_0 . Model LFs with the Minimum Mass and any e_0 agree with current observations. The good agreement of all models at $m_R \leq 20$, where the uncertainties are largest, depends on the assumed maximum radius in the model distribution. We picked 1000 km for convenience. Model LFs for $m_R \geq 20$ are independent of this choice.

To quantify the comparison between models and observations, we fit model LFs to $\log \Sigma(m_R) = \alpha(m_R - m_0)$ over $20.5 \leq m_R \leq 26.5$. Table 3 lists the fitted α and m_0 as a function of the mass in classical KBOs (in units of the Minimum Mass Solar Nebula), e_0 , the inner annulus boundary R_{in} , and the outer annulus boundary R_{out} . The small range in α for model LFs agrees with published values derived from observations². The model α is independent of the relative numbers of Plutinos and classical KBOs, and the distance distribution of classical KBOs. The observed zero-point of the LF, $m_0 \approx 23.2$ – 23.5 ,

²Gladman *et al.* (1998) report $\alpha = 0.76_{-0.11}^{+0.10}$ and $m_0 = 23.4_{-0.18}^{+0.20}$ from a maximum likelihood analysis of previous surveys with magnitude limits, $20 \leq m_R \leq 28$. Surface densities in their Table 3 yield $\alpha \approx 0.6$ and $m_0 \approx 22.4$. Jewitt *et al.* (1998; see also Luu & Jewitt 1998) quote $\alpha = 0.54 \pm 0.04$ and $m_0 = 23.2 \pm 0.10$ for $20 \leq m_R \leq 26$. Chiang & Brown (1999) prefer $\alpha = 0.52 \pm 0.02$ and $m_0 = 23.5$ for $20 \leq m_R \leq 27$; they note that the slope depends on which survey data are used in the fit.

favors models with masses comparable to the Minimum Mass Solar Nebula and any initial eccentricity. These data rule out models with $\leq 30\%$ of the Minimum Mass at the 3σ level. Smaller Plutino fractions require larger masses: if Plutinos are 10%–25% of the total KBO population, as indicated by recent observations (Jewitt *et al.* 1998), the needed mass is 2–4 times the Minimum Mass.

There are two main uncertainties in comparing our model LFs with the data, the evolution of the KBO LF with time and the current orbital parameters of KBOs. The initial mass in KBOs was larger than implied by a direct comparison between the data and model LFs, because large velocity collisions and dynamical encounters with Neptune have eroded the Kuiper Belt over time (Holman & Wisdom 1993; Davis & Farinella 1997; see also Levison & Duncan 1993; Duncan *et al.* 1995). Erosion from high velocity collisions probably does not change the slope of the LF significantly. Massive KBOs with $r_i \gtrsim 50$ km ($m_R \lesssim 26$ –27) are probably safe from collisional disruption (Davis & Farinella 1997). Disruption of smaller bodies depends on the unknown bulk properties and the poorly known orbital parameters of KBOs. These uncertainties are not important for comparisons of models and observations for $m_R \lesssim 26$ –27, but can bias future comparisons at fainter magnitude limits. Gravitational perturbations from Neptune should affect all KBO masses equally and simply reduce the total mass in KBOs with time (Holman & Wisdom 1993). Despite the uncertainty in the total amount of mass lost from the Kuiper Belt, we are encouraged that the mass needed to explain current observations of KBOs is at least the Minimum Mass Solar Nebula. Future calculations will allow us to place better constraints on the initial mass in the Kuiper Belt.

The uncertain distribution of KBO orbital parameters also affects the initial mass estimates. Our assumption of KBOs uniformly distributed in distance d_{\odot} , orbital eccentricity e , and inclination i is probably incorrect for Plutinos in specific orbital resonances with Neptune. Larger adopted volumes for current Plutinos require larger initial disk masses in the Kuiper Belt. A uniform distribution is probably reasonable for classical KBOs, but the observed range in d_{\odot} and i is not well-known. Allowing classical KBOs to occupy a larger range in semi-major axis reduces our mass estimates; a larger range in $\sin i$ increases our mass estimates. We suspect that the uncertainties currently are a factor of ~ 2 –3. Future large area surveys will provide better knowledge of KBO orbital parameters and allow more accurate models for the observed LF.

In addition to the reasonably good fit for $20.5 \leq m_R \leq 26.5$, our calculations predict 1–5 ‘Plutos’ with $m_R \leq 20$ over the entire sky. This number is uncertain, because we do not understand completely the mechanism that ends accretion and sets the maximum size of KBOs. Our calculations indicate that planetary accretion at 35–50 AU is self-limiting: once

objects reach radii of ~ 1000 km, they stir up smaller bodies sufficiently to limit additional growth. The formation of nearby Neptune should have also limited the growth of the largest bodies (Morbidelli & Valsecchi 1997). Better constraints on the radial distribution of 500+ km KBOs would test the relative importance of these two mechanisms.

Observations at fainter magnitude limits will provide additional constraints on KBO formation. Imaging data acquired at the Keck and Palomar telescopes detect KBOs with $m_R \approx 25\text{--}26.5$, where models with $e_0 \gtrsim 10^{-2}$ predict the LF to rise sharply. The apparent lack of a significant upturn in the LF at $m_R \leq 25$ implies $e_0 \lesssim$ a few $\times 10^{-2}$. In contrast, the current limit on the KBO population at $m_R \geq 28$ implies a substantial population of 10 km radius KBOs which is inconsistent with our calculations. Deeper ground-based surveys or new *HST* data could resolve the controversy surrounding this observation and place better constraints on e_0 . Finally, the proposed *Next Generation Space Telescope (NGST)* will probe the size distribution of 1 km radius KBOs where models with $e_0 \approx 10^{-3}$ predict a sharp upturn in the observed LF. If such small bodies can survive for the age of the solar system, *NGST* observations would provide important constraints on the initial mass and dynamics of the outer solar system.

We thank B. Bromley for making it possible to run our code on the JPL Cray T3D ‘Cosmos’ and the HP Exemplar ‘Neptune’ and for a generous allotment of computer time through funding from the NASA Offices of Mission to Planet Earth, Aeronautics, and Space Science. Comments from F. Franklin, M. Geller, and M. Holman greatly improved our presentation.

REFERENCES

- Aumann, H. H. *et al.*, 1984, ApJ, 278, L23
- Bailey, M. 1994, In *Asteroids, Comets, Meteors 1993*, edited by A. Milani, M. DiMartino, and A. Cellino, Kluwer Academic Publishers, Dordrecht, p. 443
- Barge, P., and Pellat, R. 1990, Icarus, 85, 481
- Boss, A. P. 1997, Science, 276, 1836
- Bowell, E., Hapke, B., Domingue, D., Lumme, K., Peltoniemi, J., and Harris, A. W. 1989, in *Asteroids II*, edited by R. P. Binzel, T. Gehrels, and M. S. Matthews, Tucson, Univ. of Arizona Press, p. 524.
- Brown, M. E., Kulkarni, S. R., & Liggett, T. J. 1997, ApJ, 490, L119
- Chiang, E. I., & Brown, M. E. 1999, AJ, 118, No. 3 (astro-ph/9905292)
- Cochran, A., Levison, H., Stern, S. A., & Duncan, M. 1995, ApJ, 455, 352
- Cochran, A. L., Levison, H. F., Tambllyn, P., Stern, S. A., & Duncan, M. 1998, ApJ, 455, L89
- Cochran, W. D., Hatzes, A. P., Butler, P. R., & Marcy, G. W. 1997, ApJ, 483, 457
- Davis, D. R., Chapman, C. R., Weidenschilling, S. J., & Greenberg, R. 1985, Icarus, 62, 30
- Davis, D. R., & Farinella, P. 1997. Icarus, 125, 50
- Davis, D. R., Ryan, E. V., & Farinella, P. 1994, Planet. Space Sci., 42, 599
- DelFosse, X., *et al.* 1998, A&A, 338, L67
- Dohnanyi, J. W. 1969, J. Geophys. Res., 74, 2531
- Duncan, M. J., & Levison, H. F. 1997, Science, 276, 1670
- Duncan, M. J., Levison, H. F., & Budd, S. M. 1995, AJ, 110, 3073
- Gladman, B., & Kavelaars, J. J. 1997, A&A, 317, L35
- Gladman, B., Kavelaars, J. J., Nicholson, P. D., Lored, T. J., & Burns, J. A. 1998, AJ, 116, 2042
- Goldreich, P., & Ward, W. R. 1973, ApJ, 183, 1051
- Greaves, J. S. *et al.* 1998, ApJ, 506, L133
- Greenberg, R., Wacker, J. F., Hartmann, W. K., & Chapman, C. R. 1978, Icarus, 35, 1

- Greenberg, R., Weidenschilling, S. J., Chapman, C. R., Davis, D. R. 1984, *Icarus*, 59, 87
- Hartmann, L., Calvet, N., Gullbring, E., & D'Alessio, P. 1998, *ApJ*, 495, 385
- Hayashi, C. 1981, *Prog Theor Phys Suppl*, 70, 35
- Holman, M. J., & Wisdom, J. 1993, *AJ*, 105, 1987
- Hornung, P., Pellat, R., & Barge, P. 1985 *Icarus*, 64, 2951
- Ida, S., & Makino, J. 1992, *Icarus*, 96, 107
- Irwin, M., Tremaine, S., & Żytkow, A. N. 1995, *AJ*, 10, 3082
- Jayawardhana, R. *et al.* 1998, *ApJ*, 503, L79
- Jewitt, D., & Luu, J. 1993, *Nature*, 362, 730
- Jewitt, D., Luu, J., & Chen, J. 1996, *AJ*, 112, 1225
- Jewitt, D., Luu, J. X., & Trujillo, C. 1998, *AJ*, 115, 2125
- Kenyon, S. J., & Luu, J. X. 1998, *AJ*, 115, 2136 (KL98)
- Kenyon, S. J., & Luu, J. X. 1999, *AJ*, 118, No. 2 (astro-ph/9904115)
- Koerner, D. W., Ressler, M. E., Werner, M. W., & Backman, D. E. 1998, *ApJ*, 503, L83
- Kokubo, E., & Ida, S. 1996, *Icarus*, 131, 171
- Kowal, C. T. 1989, *Icarus*, 77, 118
- Latham, D. W., Stefanik, R. P., Mazeh, T., Mayor, M., & Murki, G. 1989, *ApJ*, 339, 38
- Levison, H. F., & Duncan, M. J. 1990, *AJ*, 100, 1669
- Levison, H. F., & Duncan, M. J. 1993, *ApJ*, 406, L35
- Levison, H. F., & Duncan, M. J. 1997, *Icarus*, 127, 13
- Lissauer, J. J., Pollack, J. B., Wetherill, G. W., & Stevenson, D. J. 1996, in *Neptune and Triton*, edited by D. P. Cruikshank, M. S. Matthews, & A. M. Schumann, U. of Arizona Press, Tucson, 37
- Lissauer, J. J., & Stewart, G. R. 1993, In *Protostars and Planets III*, edited by E. H. Levy and J. I. Lunine, U. of Arizona Press, Tucson, p. 1061
- Luu, J. X., & Jewitt, D. 1988, *AJ*, 85, 1256
- Luu, J. X., & Jewitt, D. 1998, *ApJ*, 502, L91

- Luu, J. X., Marsden, B., Jewitt, D., Trujillo, C. A., Hergenother, C. W., Chen, J., & Offutt, W. B. 1997, *Nature*, 387, 573
- Malhotra, R. 1995, *AJ*, 110, 420
- Malhotra, R. 1996, *AJ*, 111, 504
- Marcy, G. W. 1999, in *The Physics of Star Formation and Early Stellar Evolution*, edited by C. J. Lada and N. Kylafis, Dordrecht, Kluwer, in press
- Marcy, G. W., & Butler, P. R. 1996, *ApJ*, 464, L133
- Morbidelli, A., & Valsecchi, G. B. 1997, *Icarus*, 128, 464
- Nakagawa, Y., Hayashi, C., Nakazawa, K. 1983, *Icarus*, 54, 361
- Noyes, R. W. *et al.* 1997, *ApJ*, 483, L111
- Ohtsuki, K., Nakagawa, Y., Nakazawa, K. 1988, *Icarus*, 75, 552
- Pollack, J. B., Hubickyj, O., Bodenheimer, P., Lissauer, J. J., Podolak, M., & Greenzweig, Y. 1996, *Icarus*, 124, 62
- Ruden, S. P., & Pollack, J. B. 1991, *ApJ*, 375, 740
- Russell, S. S., Srinivasan, G., Huss, G. R., Wasserburg, G. J., & Macpherson, G. J. 1996, *Science*, 273, 757
- Safronov, V. S. 1969, *Evolution of the Protoplanetary Cloud and Formation of the Earth and Planets*, Nauka, Moscow [Translation 1972, NASA TT F-677]
- Smith, B. A., & Terrile, R. J. 1984, *Science*, 226, 1421
- Stern, S. A. 1995, *AJ*, 110, 856
- Stern, S. A. 1996, *AJ*, 112, 1203
- Stern, S. A., & Colwell, J. E. 1997a, *AJ*, 114, 841
- Stern, S. A., & Colwell, J. E. 1997b, *ApJ*, 490, 879
- Weidenschilling, S. J. 1977, *Ap Sp Sci*, 51, 153
- Weidenschilling, S. J., Spaute, D., Davis, D. R., Marzari, F., Ohtsuki, K. 1997, *Icarus*, 128, 429
- Wetherill, G. W., & Stewart, G. R. 1989, *Icarus*, 77, 300
- Wetherill, G. W., & Stewart, G. R. 1993, *Icarus*, 106, 190

Williams, I. P., O'Ceallaigh, D. P., Fitzsimmons, A., Marsden, B. G. 1995, *Icarus*, 116, 180

TABLE 1. Basic Model Parameters

Parameter	Symbol	Value
Width of annulus	δa	6 AU
Initial velocity	V_0	0.45–45 m s ⁻¹
Particle mass density	ρ_0	1.5 g cm ⁻³
Relative gas velocity	η	30 m s ⁻¹
Time step	δt	1–250 yr
Number of mass bins	N	64–256
Mass spacing of bins	δ	1.25–2.0
Minimum velocity for cratering	V_f	1 cm s ⁻¹
Impact strength	S_0	2×10^6 erg g ⁻¹
Crushing energy	Q_c	5×10^7 erg g ⁻¹
Fraction of KE in ejecta	f_{KE}	0.05
Coefficient of restitution	c_1	10^{-2}
Coefficient of restitution	c_2	10^{-3}

TABLE 2. Model Results at 32–38 AU

$M_0(M_E)$	δ	e_0	q_0	τ_P (Myr)	q_f	Range (km)
1	1.4	10^{-4}	-3.0	448	-2.86 ± 0.04	2–300
10	1.4	10^{-4}	-3.0	20	-2.90 ± 0.02	1–930
1	1.4	10^{-3}	-3.0	893	-2.76 ± 0.05	6–400
3	1.4	10^{-3}	-3.0	184	-2.78 ± 0.03	5–600
10	1.4	10^{-3}	-3.0	37	-2.91 ± 0.03	6–800
30	1.4	10^{-3}	-3.0	10	-3.02 ± 0.03	6–930
100	1.4	10^{-3}	-3.0	3	-2.97 ± 0.03	7–600
10	1.4	10^{-2}	-3.0	428	-3.15 ± 0.10	50–700
100	1.4	10^{-2}	-3.0	25	-3.23 ± 0.06	20–600
10	1.25	10^{-3}	-1.5	40	-2.97 ± 0.02	7–700
10	1.25	10^{-3}	-3.0	35	-3.03 ± 0.03	9–650
10	1.25	10^{-3}	-4.5	30	-2.90 ± 0.02	4–750

TABLE 3. Luminosity Function Parameters

M_0/M_{MMSN}	e_0	R_{in} (AU)	R_{out} (AU)	α	m_0
0.3	10^{-3}	42	50	0.56 ± 0.01	24.03 ± 0.16
1.0	10^{-4}	42	50	0.58 ± 0.01	23.36 ± 0.12
1.0	10^{-3}	42	50	0.57 ± 0.02	23.16 ± 0.15
1.0	10^{-2}	42	50	0.60 ± 0.01	23.53 ± 0.18
3.0	10^{-3}	42	50	0.58 ± 0.01	22.42 ± 0.17
0.3	10^{-3}	42	60	0.56 ± 0.01	23.50 ± 0.13
1.0	10^{-4}	42	60	0.57 ± 0.01	22.85 ± 0.11
1.0	10^{-3}	42	60	0.56 ± 0.02	22.63 ± 0.13
1.0	10^{-2}	42	60	0.63 ± 0.02	23.31 ± 0.19
3.0	10^{-3}	42	60	0.58 ± 0.01	21.92 ± 0.17

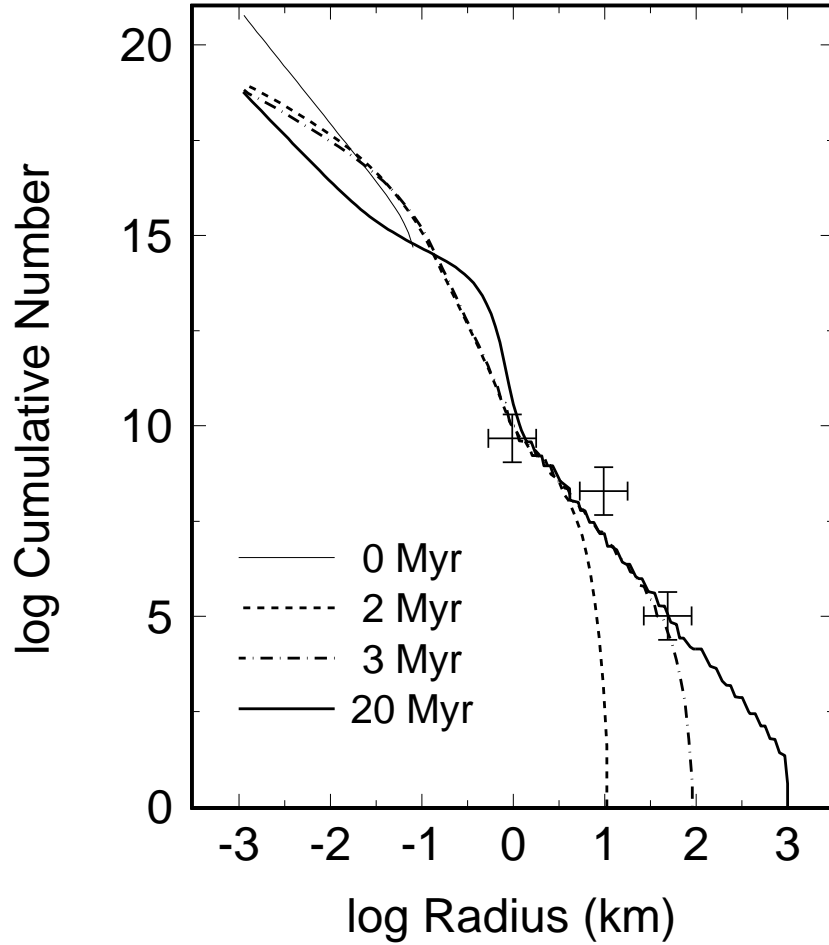


Fig. 1.— Cumulative size distributions as a function of time for a model with $M_0 = 10M_E$ and $e_0 = 10^{-4}$. The evolution time for each curve is listed in the legend. Crosses indicate observational and theoretical constraints on the size distribution at radii of 50 km, 10 km, and 1 km as described in the text.

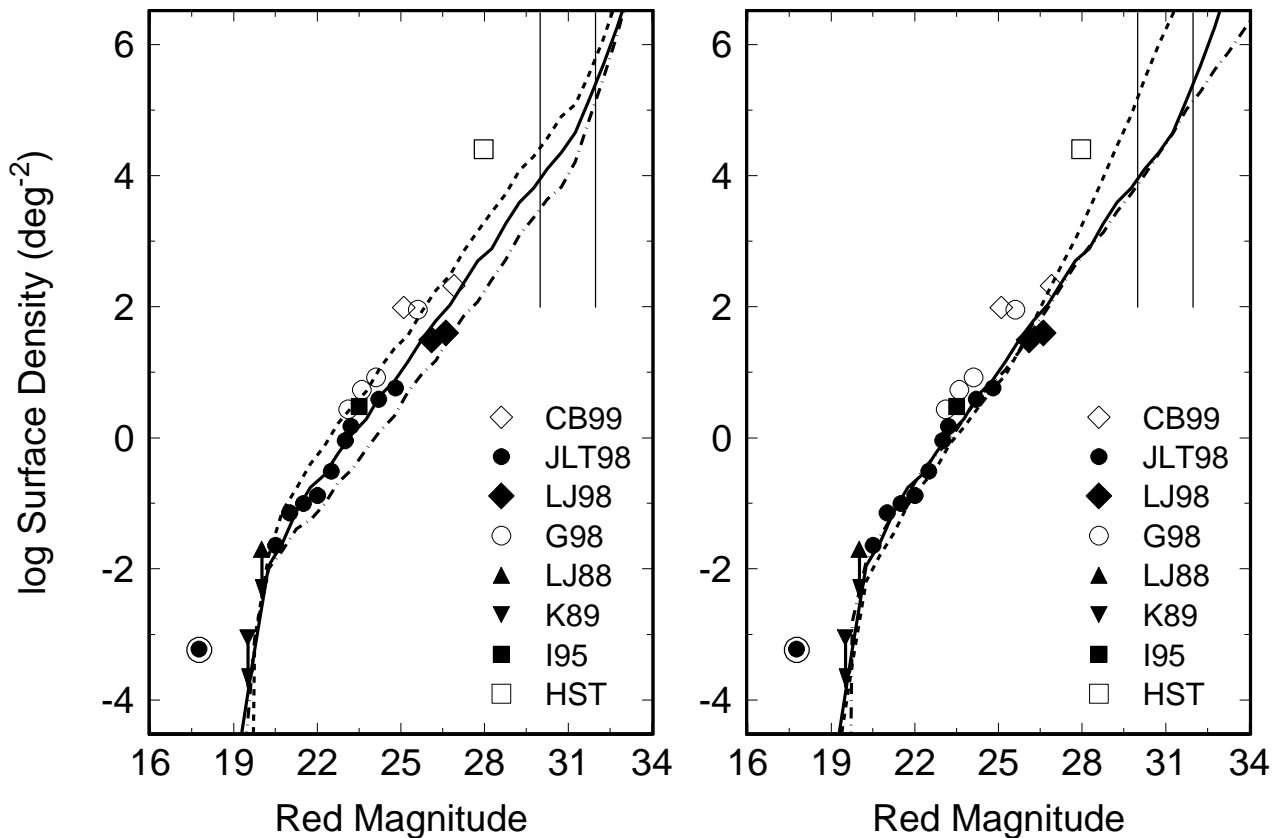


Fig. 2.— Comparison of model luminosity functions of KBOs with observations. Data are as indicated in the legend of each panel. The open circle with the central dot is the position of Pluto for an adopted albedo of 4%; other observations are from Cochran *et al.* (1998; HST), Irwin *et al.* (1995; I95), Kowal 1989 (1989; K89), Luu & Jewitt (1988; LJ88), Gladman *et al.* (1998; G98), Luu & Jewitt (1998; LJ98), Jewitt *et al.* (1998; JLT98) and Chiang & Brown (1999; CB99). Error bars for each datum – typically a factor of 2–3 – and the upper limit from Levison & Duncan (1990) are not shown for clarity. The lines plot luminosity functions for models with (a) left panel: $e_0 = 10^{-3}$ and $M_0 \approx 0.3$ (dot-dashed), 1.0 (solid), and 3.0 (dashed) times the Minimum Mass Solar Nebula and (b) right panel: a Minimum Mass Solar Nebula with $e_0 = 10^{-2}$ (dashed), $e_0 = 10^{-3}$ (solid), and $e_0 = 10^{-4}$ (dot-dashed). A Minimum Mass Solar Nebula has $M_0 \approx 12 M_E$ within $R = 42\text{--}50$ AU. The pair of vertical solid lines indicates the planned magnitude range accessible to *NGST*.